J. Electrochem. Sci. Eng. **13(4)** (2023) 659-672; http://dx.doi.org/10.5599/jese.1558

Open Access : : ISSN 1847-9286
www.jESE-online.org

Original scientific paper

Predicting the effect of silicon electrode design parameters on thermal performance of a lithium-ion battery

Harika Dasari✉ and Eric Eisenbraun

SUNY Polytechnic Institute, College of Nanoscale Science and Engineering, Albany, NY 12203, USA

Corresponding author: ✉dasarih@sunypoly.edu

Received: October 21, 2022; Accepted: January 12, 2023; Published: February 20, 2023

Abstract

The present study models the role of electrode structural characteristics on the thermal behaviour of lithium-ion batteries. Preliminary modelling runs have employed a 1D lithium-ion battery, coupled to a two-dimensional axisymmetric model using silicon as the battery anode material. The two models are coupled by the heat generated and the average temperature. Our study is focused on the silicon anode particle sizes, and it is observed that silicon anodes with nano sized particles reduced the heating of the battery under charge/discharge cycles when compared to anodes with larger particles. These results are discussed in context of the relationship between particle size and thermal transport properties in the electrode.

Keywords

Particle size, lithium nickel manganese cobalt oxide, heat generation, separator

Introduction

Lithium-ion batteries, which possess relatively high energy and power densities, are useful in many fields including electric vehicles and aerospace applications. Electric vehicles require high energy and power density to ensure both maximum mileage and maximum travel speed. A trade-off exists between energy and power density in batteries and most research is focused on the simultaneous improvement of both characteristics [1,2]. While graphite is widely used as an anode material in lithium-ion batteries, silicon (Si) can be considered as an electrode material since it possesses good electrochemical properties and high theoretical, volume specific capacity as shown in Table 1. However, Si is susceptible to failure mechanisms like large volume changes during lithiation, decomposition of the solid electrolyte interface (SEI) layer, and low conductivity; consequently, capacity fade is also observed [3,4].

Employing nanostructured silicon particles as the active material for the negative electrode is one of the best ways to overcome the above-mentioned problems. Such structures reduce mechanical stresses which cause volume changes. In our previous research work, we observed that negative electrode particle size in nanometers improved capacity when compared to particle size in micrometers [5].

Table 1. *Properties of graphite and silicon anodes [6-7]*

Anode material	Graphite	Silicon
Lithiated phase	LiC_6	$Li_{4,4}$ Si
Theoretical specific capacity, mAh g^{-1}	372	4200
Theoretical volume capacity, mAh cm^{-3}	837	9786
Volume change, %	12	320

Apart from studies of capacity fade, it is also important to understand the thermal behavior of nano-structured silicon particles. In general, the heat generated in a battery is classified as reversible heat and irreversible heat. While reversible heat originates from the entropy changes of the active materials of the electrode, irreversible heat is created from other processes which occur in the battery [8].

There are two sources of irreversible heat: polarization heat, which is formed due to the overpotential, and ohmic heat, resulting from the resistance due to the movement of Li^+ during the electrochemical reaction process [8].

The electrode is the most important component of a battery, as it affects the capacity, power density, and energy density, and defines the quantity and speed of lithium storage within the battery. Therefore, approaches like selecting appropriate materials, *e.g.*, using different mixed cathode materials, altering the ratio of active to inactive materials, or optimizing battery design parameters of the electrodes such as particle size, electrode thickness, volume fraction, and other factors are typically considered for electrode design [8-18].

The most widely used separators are comprised of a polymer matrix embedded in the electrolyte solution. This electrolyte solution is a liquid with salts dissolved in water or organic solvents.

Poly (vinylidene fluoride-co-hexafluoropropylene) p(VdF-HFP) exhibits high polarity, good thermal and mechanical properties, and wettability by organic solvents. They are chemically stable and inert and possess porosity that is tailorable even through binary and ternary solvent or non-solvent systems, therefore, we have used it as the separator material for our current model [19].

To quantify the impact of specific design variables on cell heat generation and electric performance in lithium-ion batteries, parametric studies were carried out using higher fidelity models. A coupled electrochemical-thermal model was developed by Wu *et al.* [20] and Bin Huang *et al.* [21] to study the impact of electrode thickness and particle size on heat generation rate and battery performance [20] in cylindrical batteries [21]. A new modeling framework was employed by Madsen *et al.* [22] to study the effect of design parameters like particle sizes on heat generation and battery performance. C-rate is a unit used to measure the rate at which a battery is fully charged or discharged relative to its capacity. At higher C-rates, smaller size electrode particles lead to a higher battery capacity in charge and discharge cycles. Larger particle sizes and higher C-rates also increase overpotential in a battery [23]. These studies quantified the impact of various parameters in electrodes on heat generation of the battery where the effect of particle size was not monotonic across the discharge rates and the larger particle sizes increased heat generation and potential sweep rate.

Increasing the volume fraction of electrolyte in the electrodes will result in a large amount of Li^+ intercalation and deintercalation in the electrode, subsequently increasing the capacity fade, internal resistance, and polarization, resulting in a larger gradient of electrochemical properties and a higher rate of heat generation. Hence, we chose the optimized volume fraction value that we obtained in our former work as 0.45 for the current model [5].

Though the electrochemical behavior of silicon is well studied, most of the work is focused on half-cells with Li metal as a counter electrode which cannot address the long-term cycling performance of silicon anodes [24]. The current work is focused on electrochemical modeling where we studied the

effects of different particle sizes of the silicon electrode on the temperatures of the battery. For this purpose, we have used a full-cell configuration in our simulations where we have used a lithium nickel manganese cobalt oxide (NMC) cathode. In our previous work [5] NMC cathode has shown an improved relative capacity with a silicon anode, so we have used the same cathode in this work to understand its behavior with a silicon anode. A cylindrical structure was modeled to understand electronic current conduction in the electrodes and ionic charge transport in the electrodes and electrolyte/separator.

Methods

Model development

The current cylindrical 2D Thermal model employs heat transfer across a solid interface and has axial symmetry. It uses silicon as the negative electrode, $LiNi_{1/3}Mn_{1/3}Co_{1/3}O_2$ (NMC 111) as the positive electrode, and LiPF6 in 2:1 EC: DMC and poly (vinylidene fluoride-co-hexafluoropropylene) p(VdF-HFP) as the separator. In a spirally wound battery, heat conduction in the spiral direction is not considered and wound sheets are modeled as one active battery material domain [25] as shown in Fig 1.

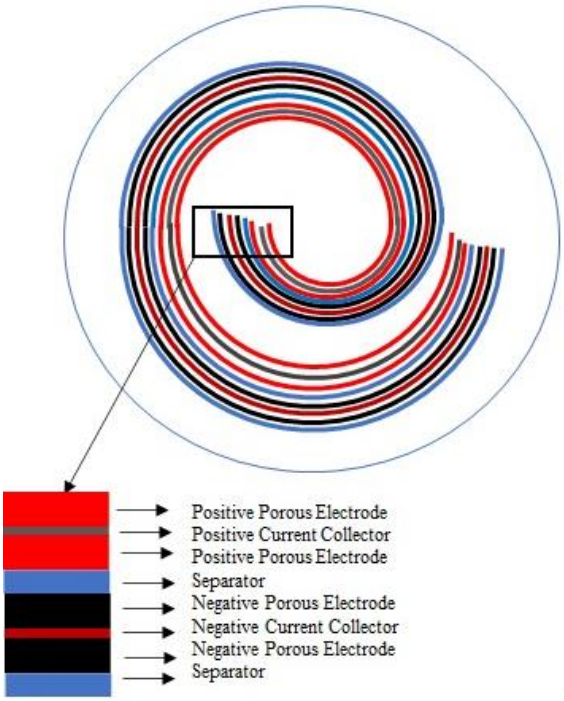

Figure 1. *Layered spiral geometry of a cylindrical battery [25]*

Model equations

The cylindrical battery geometry (9 mm radius, 65 mm height) consists of three domains (shown in Fig. 2): Battery canister (steel, 0.25 mm thick), Active battery material domain (wound sheets of cell material, 55 μm), Mandrel (isolator around which the battery cell sheets are wound, 2 mm radius). The initial state of charge of the battery is 20 %.

The active material of the battery consists of several battery cells wound spirally into a cylinder. The current model has higher thermal conductivity along the battery sheets, which is in the cylinder length direction, and lower in the normal direction to the sheets, the radial direction [25].

The thermal conductivity in the radial direction, $k_{T,r}$ is calculated by Eq. (1):

$$k_{T,r} = \frac{\sum L_i}{\sum \frac{L_i}{k_{T,i}}} \quad (1)$$

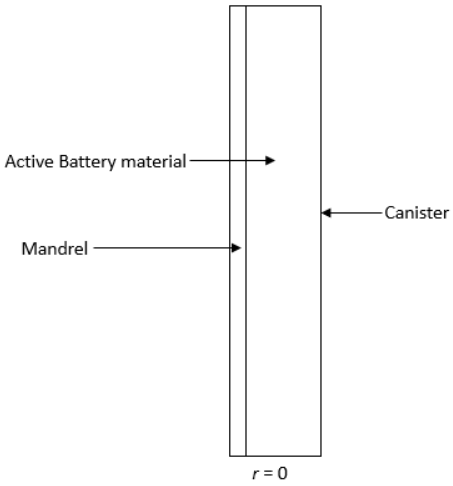

Figure 2. *Cross-sectional cutaway view of the geometry of thermal model battery [25]*

Thermal conductivity in the cylinder length direction, $k_{T,ang}$ is determined by Eq. (2):

$$k_{T,ang} = \frac{\sum L_i k_{T,i}}{L_i} \quad (2)$$

The density of the active battery material is calculated by Eq. (3):

$$\rho_{batt} = \frac{\sum L_i \rho_i}{\sum L_i} \quad (3)$$

Similarly, the heat capacity of the active material is as given in Eq. (4):

$$C_{p,batt} = \frac{\sum L_i C_i}{\sum L_i} \quad (4)$$

Governing equations, boundary conditions, and parameters used in the modeling are taken from the COMSOL material library [25]. Material dependent thermal parameters are from published research works [26-28]. Tables 2 and 3 describe the dimensions of the electrode, separator, and thermal parameters of the battery components. We have listed the various particle sizes considered in our model as case studies in Table 4.

Table 2. *Electrochemical parameters of the model [25]*

Parameter	Symbol	NMC	Silicon	Separator
Solid phase Li-diffusivity negative, $m^2 s^{-1}$	D_{s_neg}		$3.9\ 10^{-14}$	
Solid phase Li-diffusivity positive, $m^2 s^{-1}$	D_{s_pos}	10^{-13}		
Max solid phase concentration negative, mol m^{-3}	c_{smax_neg}		278000	
Max solid phase concentration positive, mol m^{-3}	c_{smax_pos}	49000		
Volume fraction of the active material	$\varepsilon_{s,1}$, $\varepsilon_{s,2}$	0.30	0.45	
Electrolyte salt concentration, mol m^{-3}	c_0			2000
Particle size, nm	r_P	Varied	Varied	
Reaction rate coefficient negative, $m^2 s^{-1}$	k_{neg}		$2\ 10^{-11}$	
Reaction rate coefficient positive, $m^2 s^{-1}$	k_{pos}	$2\ 10^{-11}$		
Positive electrode density, kg m^{-3}	ρ_{pos}	2328.5		
Negative electrode density, kg m^{-3}	ρ_{neg}		1347.33	
Length of the negative electrode, μm	L_{neg}		55	
Length of the positive electrode, μm	L_{pos}	55		
Length of separator, μm	L_{sep}			30
Charge transfer coefficient	α	0.5	0.5	
Bruggeman coefficient	γ	1.5	1.5	
Transference number	t_+			0.363
Specific surface area	$a_{s,i}$	Eq. (9)	Eq. (9)	
Average molar activity coefficient	f		0	

Table 3. *Thermal parameters of the model*

Thermal parameters	Symbol	Values
Positive current collector density, kg m^{-3}	ρ_{pos_cc}	2770
Negative current collector density, kg m^{-3}	ρ_{neg_cc}	8933
Separator density, kg m^{-3}	ρ_{sep}	1008.98
Positive electrode heat capacity, J kg^{-1} K^{-1}	C_{pos}	1270
Negative electrode heat capacity, J kg^{-1} K^{-1} [26,27]	C_{neg}	680
Positive current collector heat capacity, J kg^{-1} K^{-1}	C_{pos_cc}	875
Negative current collector heat capacity, J kg^{-1} K^{-1}	C_{neg_cc}	385
Separator heat capacity	C_{sep}	1978.16
Negative electrode thermal conductivity, W mK^{-1} [28]	k_{T_neg}	156
Positive electrode thermal conductivity, W mK^{-1}	k_{T_pos}	1.58

Table 4. *Test cases used for simulations*

Case study	r_P / μm	
	NMC	Silicon
Case 1	8.0	12.5
Case 2	8.0	0.100
Case 3	0.100	2.000
Case 4	0.100	0.100

Results and discussion

The electrochemical-thermal model was resolved using COMSOL Multiphysics version 5.6 software. Fig. 3 shows the temperature distribution in the battery for a silicon electrode particle radius of 12.5 μm and NMC electrode particles 8 μm for case study 1. The temperature - time graphs in Fig. 4 show that the peak temperature change in the battery over 2000 seconds charging and discharging cycle is 13 K. The temperature-time graphs show slope changes up to 1500 seconds at various points of time representing charging/discharging in the battery. The battery is charged until 300 seconds, followed by discharge until 600 seconds then charged again until 900 seconds and discharged until 1200 seconds, and then it is charged until 1500 seconds. At 1500 seconds, an open circuit voltage (or when the battery is disconnected) results in a fall in the temperature. The individual curves represent the maximum, minimum, and mean temperatures of the battery. Similarly, Fig. 5 shows the temperature distribution of the battery where the silicon electrode particle radius is 100 nm and NMC electrode particles 8 μm for case study 2. Fig. 6 shows the peak temperature change is 11.5 K in the battery for silicon electrode particle radius is 100 nm and NMC electrode particles 8 μm.

Fig. 7 and Fig. 9 show the temperature distributions in the battery for silicon electrode particle radii of size 2000 nm and 100 nm, with constant particle sizes of 100 nm of NMC respectively for case study 3 and case study 4. Similarly, Fig. 8 and Fig. 10 show that when the silicon electrode particle radii are 2000 nm and 100 nm, the peak temperature changes in the battery were 8.8 and 7.5 K, respectively.

The increasing temperatures during charging/discharging were due to ohmic heating and entropy changes in the battery [25]. The differences between the maximum and minimum temperatures would not exceed 3 K using the current thermal modeling. Entropy effects or reversible heating contributes to the heating rate difference between the charge and discharge in the battery.

The temperature change was higher for larger (micron scale) particle sizes than the nanometer-sized particles. Hence, nanoparticles reduce the temperature variations in a battery when compared to micro-sized particles. These results are summarized in Table 4.

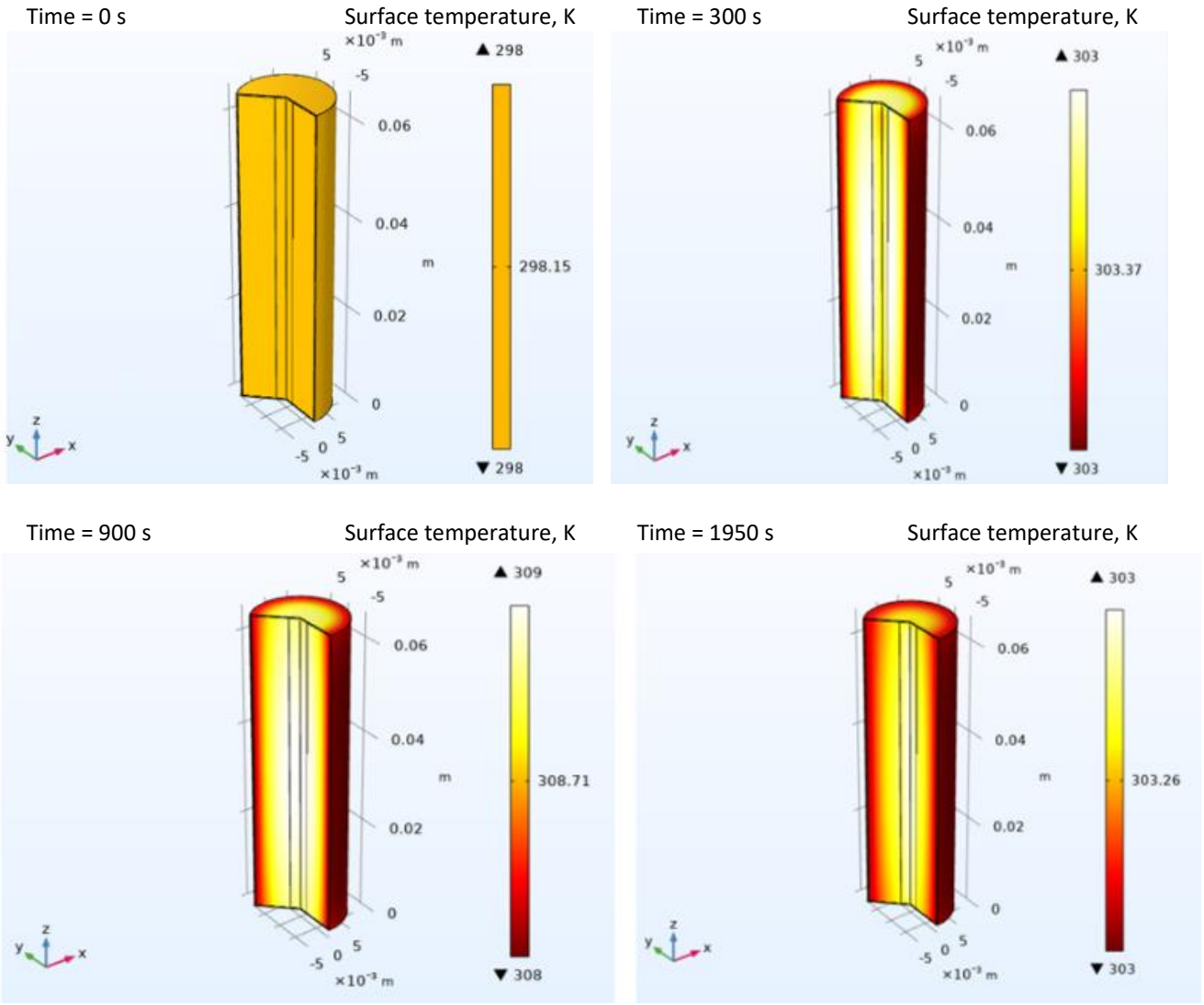

Figure 3. *Simulated comparison of temperature distribution in the battery at different time periods when the radius of the negative electrode particles is 12.5 μm and NMC electrode particles 8 μm (Case 1)*

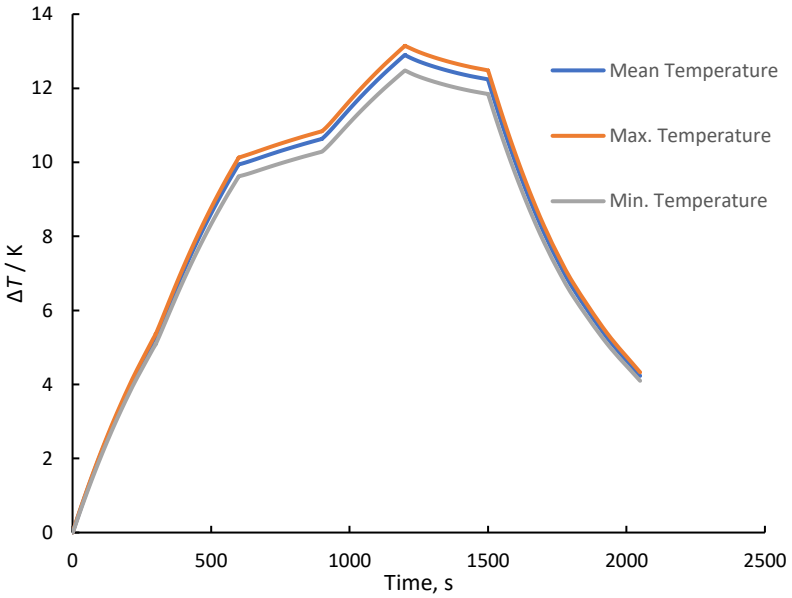

Figure 4. *Temperature* vs. *time when the radius of the negative electrode particles is 12.5 μm and NMC electrode particles 8 μm (Case 1)*

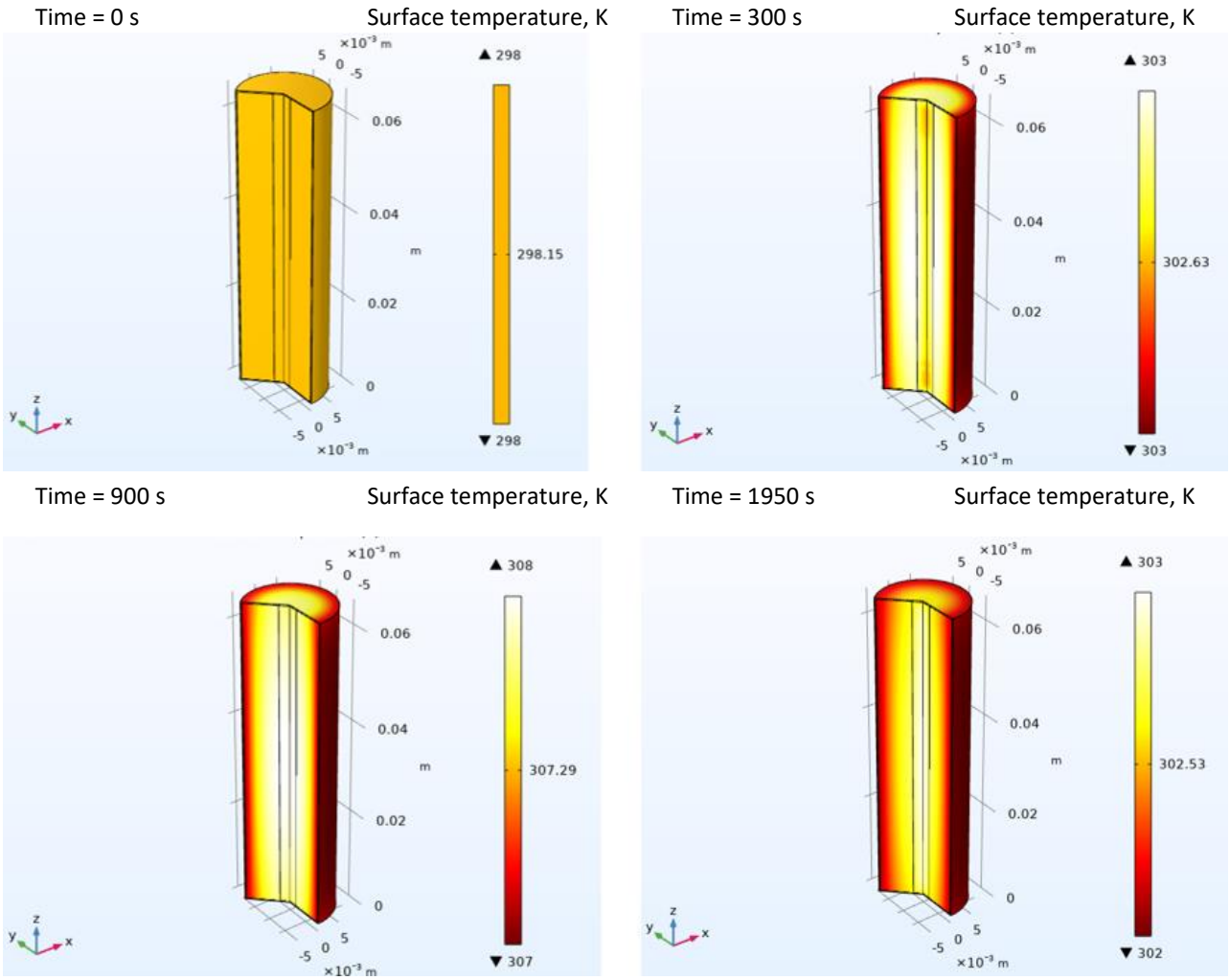

Figure 5. *Simulated comparison of temperature distribution in the battery at different time periods when the radius of the negative electrode particles is 100 nm and NMC electrode particles 8 μm (Case 2)*

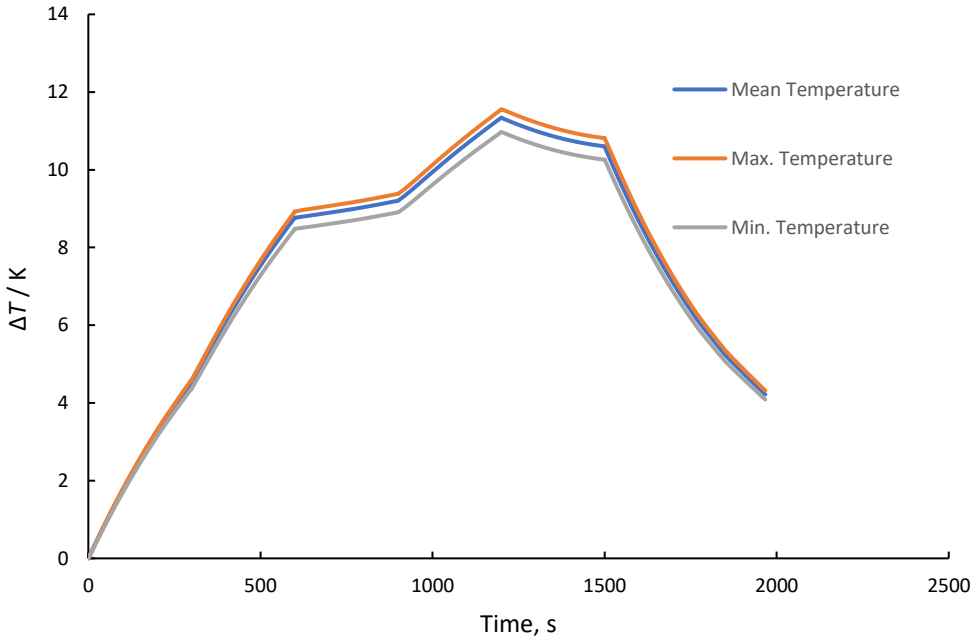

Figure 6. *Temperature* vs. *time when the radius of the negative electrode particles is 100 nm and NMC electrode particles 8 μm (Case 2)*

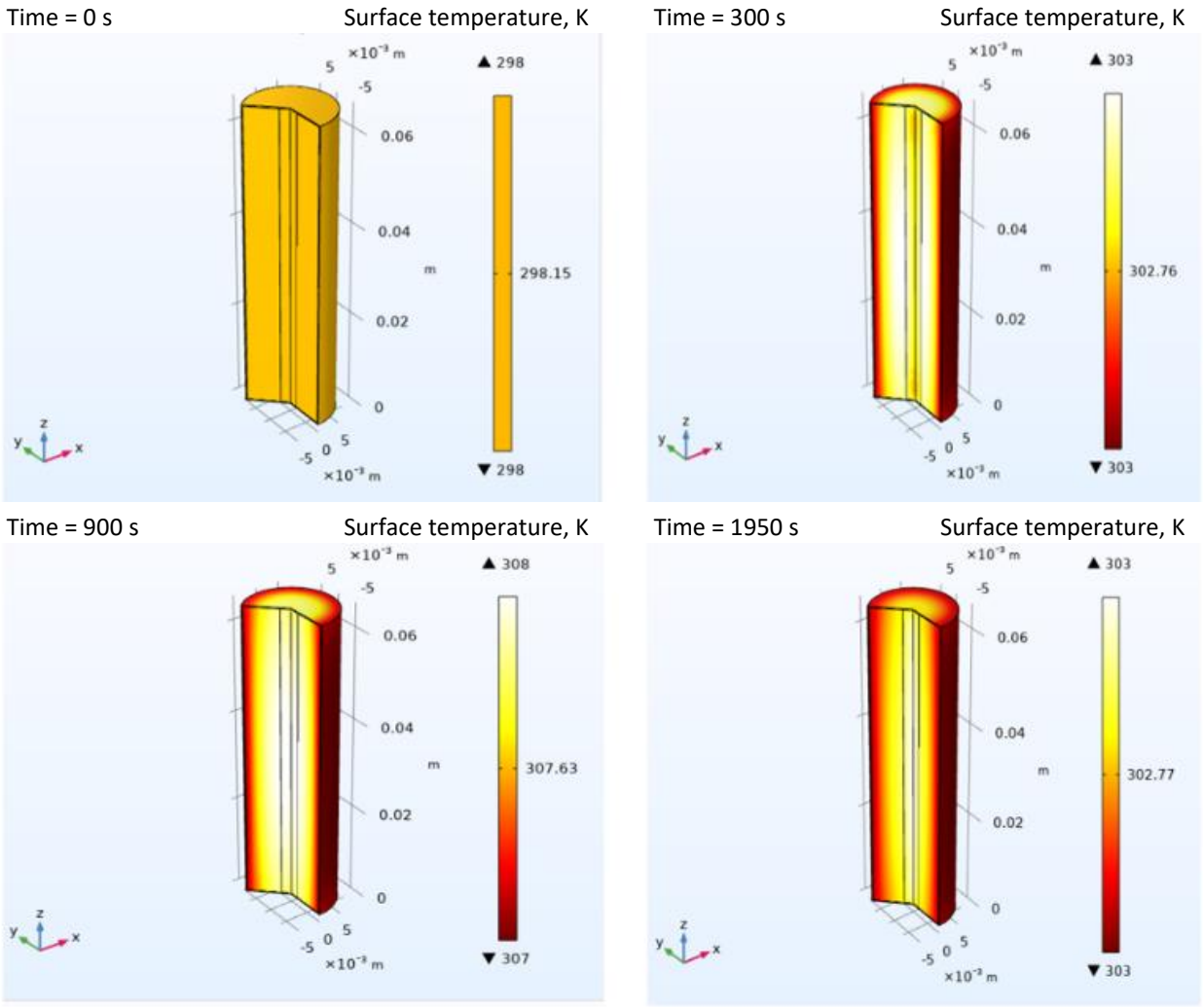

Figure 7. *Simulated comparison of temperature distribution in the battery at different time periods when the radius of the negative electrode particles is 2000 nm (Case 3)*

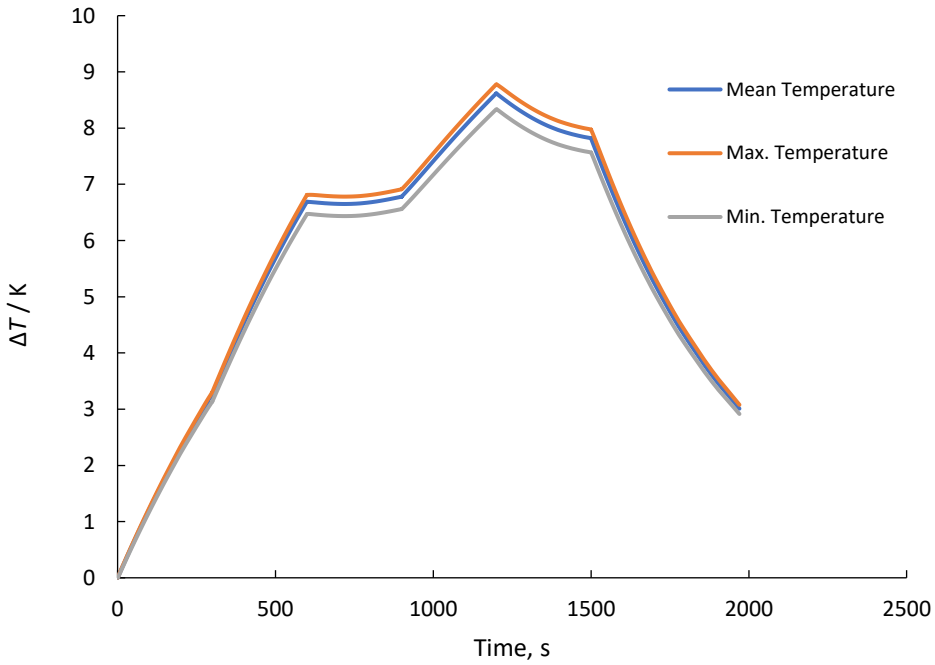

Figure 8. *Temperature* vs. *time when the radius of the negative electrode particles is 2000 nm (Case 3)*

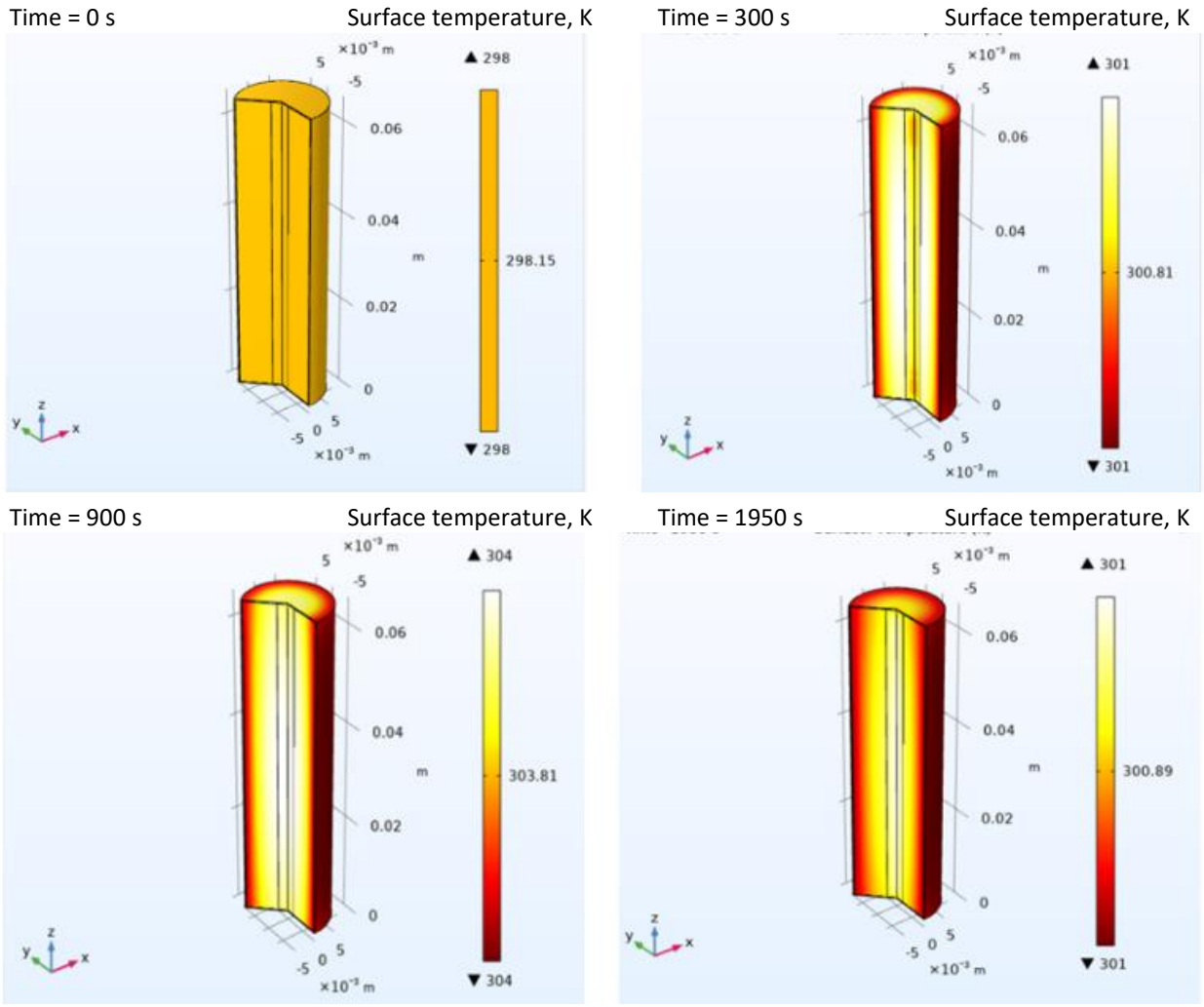

Figure 9. *Simulated comparison of temperature distribution in the battery at different time periods when the radius of the negative electrode particles is 100 nm (Case 4)*

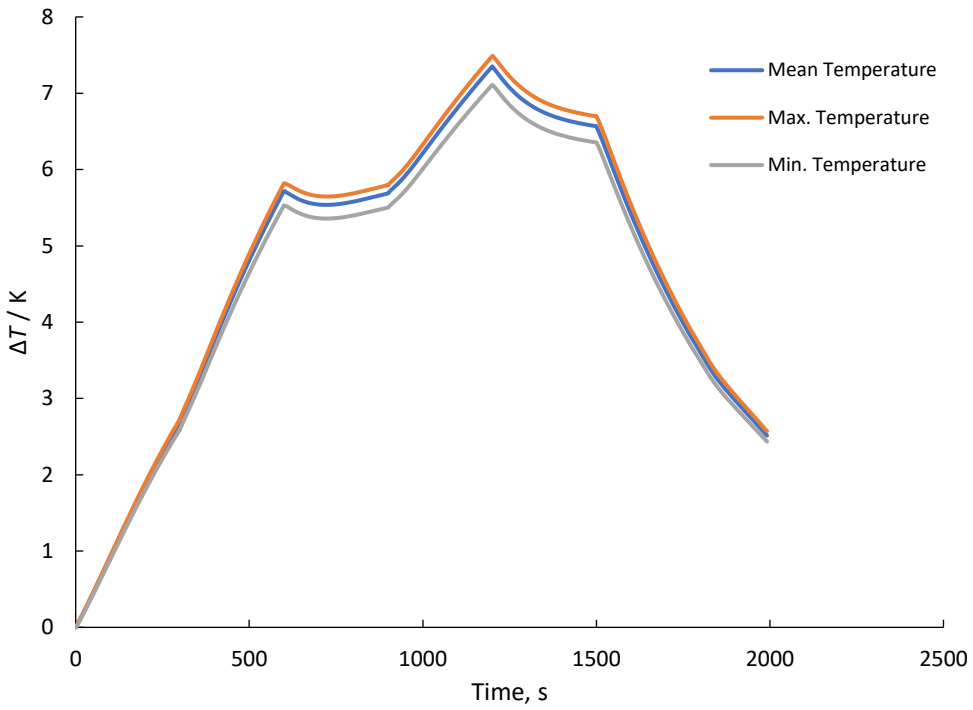

Figure 10. *Temperature vs. time when the radius of the negative electrode particles is 100nm (Case 4)*

Table 4. *Simulation results of the test cases*

Case study	r_P / μm		Peak temperature, K
	NMC	Silicon	
Case 1	8.0	12.5	13
Case 2	8.0	0.100	11.5
Case 3	0.100	2.000	8.8
Case 4	0.100	0.100	7.5

Heat generation

The heat generation rate is dependent on the battery chemistry and kinetics. These factors influence heat generation, which greatly varies with the battery design. The battery chemistry is well defined for a battery system with a defined range of operating conditions. Battery design parameters and operating conditions define the kinetics of the battery system. The following equations are involved in battery kinetics.

The energy conservation in the battery occurs according to Eq. (5) [8]:

$$\rho C_p \frac{\partial T}{\partial t} = \lambda_x \frac{\partial^2 T}{\partial x^2} + \lambda_y \frac{\partial^2 T}{\partial y^2} + \lambda_z \frac{\partial^2 T}{\partial z^2} + q \quad (5)$$

where,

ρ / kg m^{-3} = density

C_p / J kg^{-1} K^{-1} = heat capacity

λ / W m^{-1} K^{-1} = thermal conductivity

$q = q_{rev} + q_{irrev}$; $q_{irrev} = q_{ohm} + q_{act}$

where,

q / W m^{-3} = heat generation rate

q_{rev} / W m^{-3} = reversible heat

q_{irrev} / W m^{-3} = irreversible heat

q_{ohm} / W m^{-3} = ohmic heat

q_{act} / W m^{-3} = polarization heat

Ohmic heat is created by the resistance to the flow of electrons in the solid phase and lithium ions in the electrolyte phase. Ohmic heat is calculated by Eq. (6) [8,29]:

$$q_{ohm} = -i_s \nabla \Phi_s - i_l \nabla \Phi_l \quad (6)$$

Where Φ_s is electric potential which is the potential energy difference per unit charge between two points in an electric field and Φ_l is the electrolyte potential is the potential of electrochemical species in a solution.

$$i_s = -\sigma_s \nabla \Phi_s \quad (7)$$

where σ_s is the electrical conductivity.

Polarization heat is dependent on the sizes of the active material particles and the overpotential generated in the battery. It increases with the particle sizes of the electrodes, and it is calculated by Eq. (8):

$$q_{act} = a_s i_{loc} \eta \quad (8)$$

where a_s is specific interfacial area of the porous electrode or specific surface area, Eq. (9)

$$a_s = 3\varepsilon_s / r \quad (9)$$

r / m = radius distance variable of the solid particles

η = overpotential.

Butler - Volmer equation is used for the local current density calculation, Eqs. (10) and (11):

$$i_{loc} = i_0 \left(e^{\frac{\alpha_a F \eta}{RT}} - e^{\frac{\alpha_c F \eta}{RT}} \right) \quad (10)$$

$$i_0 = F k_c^{\alpha_a} k_c^{\alpha_c} \left(c_{s,max} - c_s \right)^{\alpha_a} c_s^{\alpha_a} \frac{c_l}{c_{l,eff}} \quad (11)$$

where α_a and α_c are the anode and cathode transfer coefficients and k_a and k_c are the reaction rate constants for the anode and cathode.

Reversible heat in the electrodes is caused due to entropy changes and is as given in Eq. (12):

$$q_{rew} = a_s i_{loc} T \frac{\partial U}{\partial t} \quad (12)$$

where, $\partial U / \partial t$ *is* potential deviation of the electrodes resulting from entropy changes.

The charge and mass conservation in the solution phase happen according to Eqs. (13) to (16):

$$i_l = -\sigma \nabla \Phi_l + \frac{2\sigma_l RT}{F} \left(1 + \frac{\partial \ln f}{\partial \ln c_l} \right) (1 - t_+) \nabla \ln c_l \quad (13)$$

$$R_l - \frac{i_{tot} + Q_l}{F} t_+ = \varepsilon_l \frac{\partial c_l}{\partial t} + \nabla \left(D_l \nabla C_l \right) \quad (14)$$

$$\nabla i_l = i_{tot} + Q_l \quad (15)$$

Charge conservation in solid phase, Eq. (16):

$$\nabla i_s = -i_{tot} + Q_s \quad (16)$$

Mass balance of Li in the particles is determined by Eq. (17):

$$\frac{\partial c_s}{\partial t} = \nabla \left(D_s \nabla c_s \right) \quad (17)$$

where c_s is the concentration of Li in solid phase, D_s is solid phase Li diffusion coefficient.

Some of the temperature-dependent parameters include electrolyte conductivity, the diffusion coefficient of electrolyte, and the potential deviation of the electrodes [8,29]. These parameters influence the temperature versus time graphs in each case study, leading to discontinuities in the temperature curves. As shown in the above formulas, polarization heat and reversible heat are dependent on the size of the active electrode particles. Decreasing the particle sizes decreases polarization heat and reversible heat in the battery.

A reduction in particle size leads to an increase in the specific surface area. Specific surface area is one of the contributing factors in the reduction of solid phase diffusion polarization. It was observed that, as the particle size decreased, the heat generation in the battery decreased. The reason behind the phenomenon is that the particle size influences the solid phase diffusion polarization [8]. When the electrode active material particle sizes are smaller, they provide shorter distances for insertion and de-insertion. Consequently, the larger specific surface area of smaller particles ensures lower surface current density which leads to a decrease in solid phase diffusion polarization [8]. Most of the published research works were focused on how electrode particle sizes effect overpotential, capacity and the heat generation rate [23]. Our work estimated the temperature change with respect to time and different particle sizes of the negative electrode.

Conclusion

Our current full cell model found that Si anodes with nano-sized particles reduce the temperature of the battery compared to larger particles in Li-ion batteries. The primary reason for this observed behavior is believed to be that Li^+ ions take less time to diffuse across smaller particles and hence lead to a smaller increase in the battery temperature. Reduction in the diffusion length of lithium-

ion in the insertion or extraction process by nanoparticles enhances the rate performance of the electrode material, thus increasing the capacity and overall performance of lithium-ion batteries.

List of symbols and abbreviations

a_s / m^2 m^{-3}	Specific surface area
i_l / A m^{-2}	Electronic current density in the solid phase
Q_l	Electrolyte current source
i_{tot}	The sum of all electrochemical current sources
c_l / mol m^{-3}	Electrolyte salt concentration
f	Average molar activity coefficient
Q_s	Current source term
R_l	Total Li^+ source term in the electrolyte
R / m	Radius distance variable of the solid particles
i_{loc} / A m-^{2}	Local current density
i_0 / A m-^{2}	Exchange current density
T / K	Battery temperature
R	Gas constant, 8.314 J mol^{-1} K^{-1}
σ_l / S m^{-1}	Electronic conductivity of solid phase
σ_s / S m^{-1}	Ionic conductivity of the electrolyte
$\varepsilon_{1,s}$	Solid phase volume fraction of the negative electrode
$\varepsilon_{2,s}$	Solid phase volume fraction of the positive electrode
$\varepsilon_{1,e}$	Electrolyte phase volume fraction negative electrode
$\varepsilon_{2,e}$	Electrolyte phase volume fraction positive electrode
ε_l	Electrolyte volume fraction
ε_s	Electrode volume fraction
η	Overpotential
F	Faraday's constant, 96 487 C mol^{-1}

Subscripts

l	Solution phase
s	Solid phase
eff	Effective value of transport property in porous medium

References

[1] C. Liu, L. Liu, Optimal Design of Li-Ion Batteries through Multi-Physics Modeling and Multi-Objective Optimization, *Journal of The Electrochemical Society* **164(11)** (2017) E3254-E3264. https://doi.org/10.1149/2.0291711jes

[2] M. J. Lain, J. Brandon, E. Kendrick, Design Strategies for High Power *vs.* High Energy Lithium Ion Cells, *Batteries* **5(4)** (2019) 64. https://doi.org/10.3390/batteries5040064

[3] M. Ge, X. Fang, J. Rong, V. Zhou, Review of porous silicon preparation and its application for lithium-ion battery anodes, *Nanotechnology* **24(42)** (2013) 422001. https://doi.org/10.1088/0957-4484/24/42/422001

[4] M. Salah, P. Murphy, C. Hall, C. Francis, R. Kerr, M. Fabretto, Pure silicon thin-film anodes for lithium-ion batteries, *Journal of Power Sources* **414** (2019) 48-67. https://doi.org/10.1016/j.jpowsour.2018.12.068

[5] H. Dasari, E. Eisenbraun. Predicting Capacity Fade in Silicon Anode-Based Li-Ion Batteries, *Energies* **14** (2021) 1448. https://doi.org/10.3390/en14051448

[6] P. U. Nzereogu, A. D .Omah, F. I. Ezema, E. I. Iwuoha, A. C. Nwanya, Anode materials for lithium-ion batteries, *Applied Surface Science Advances* **9** (2022) 100233. https://doi.org/10.1016/j.apsadv.2022.100233

[7] X. Song, X. Wang, Z. Sun , P. Zhang , L. Gao, Recent developments in silicon anode materials for high performance lithium-ion batteries, *Material Matters* **8** (2016). https://www.sigmaaldrich.com/US/en/technical-documents/technical-article/materials-science-and-engineering/batteries-supercapacitors-and-fuel-cells/recent-developments-in-silicon-anode-materials.

[8] W. Mei, H. Chen, J. Sun, Q. Wang, The effect of electrode design parameters on battery performance and optimization of electrode thickness based on the electrochemical-thermal coupling model, *Sustainable Energy & Fuels* **3** (2019) 148-165. https://doi.org/10.1039/C8SE00503F

[9] K. Kisu, S. Aoyagi, H. Nagatomo, E. Iwama, M. T. H. Reid, W. Naoi and K. Naoi, Internal resistance mapping preparation to optimize electrode thickness and density using symmetric cell for high-performance lithium-ion batteries and capacitors, *Journal of Power Sources* **396** (2018) 207-212. https://doi.org/10.1016/j.jpowsour.2018.05.083

[10] Y. H. Chen, C. W. Wang, X. Zhang, A. M. Sastry, Porous cathode optimization for lithium cells: ionic and electronic conductivity, capacity, and selection of materials, *Journal of Power Sources* **195(9)** (2010) 2851-2862. https://doi.org/10.1016/j.jpowsour.2009.11.044.

[11] H. Zheng, R. Yang, G. Liu, X. Song, V. S. Battaglia, Cooperation between Active Material, Polymeric Binder and Conductive Carbon Additive in Lithium-Ion Battery Cathode, *The Journal of Physical Chemistry C* **116(7)** (2012) 4875-4882. https://doi.org/10.1021/jp208428w

[12] J. W. Fergus, Recent developments in cathode materials for lithium-ion batteries *Journal of Power Sources* **195(4)** (2010) 939-954. https://doi.org/10.1016/j.jpowsour.2009.08.089.

[13] C. H. Lu, S. W. Lin, Influence of the particle size on the electrochemical properties of lithium manganese oxide, *Journal of Power Sources* **97-98** (2001) 458-460. https://doi.org/10.1016/S0378-7753(01)00637-1.

[14] L. Xiao, Y. Guo, D. Qu, B. Deng, H. Liu, D. Tang, Influence of particle sizes and morphologies on the electrochemical performances of spinel $LiMn_2O_4$ cathode materials, *Journal of Power Sources* **225** (2013) 286-292. https://doi.org/10.1016/j.jpowsour.2012.10.070

[15] R. Zhao, J. Liu, J. Gu, The effects of electrode thickness on the electrochemical and thermal characteristics of lithium-ion battery, *Applied Energy* **139** (2015) 220-229. https://doi.org/10.1016/j.apenergy.2014.11.051

[16] H. Zheng, J. Li, X. Song, G. Liu, V. S. Battaglia, A comprehensive understanding of electrode thickness effects on the electrochemical performances of Li-ion battery cathodes, *Electrochimica Acta* **71** (2012) 258-265. https://doi.org/10.1016/j.electacta.2012.03.161

[17] J. Newman, Optimization of Porosity And Thickness of a Battery Electrode by Means of a Reaction-Zone Model, *Journal of The Electrochemical Society* **142(1)** (1995) 97-101. https://doi.org/10.1149/1.2043956

[18] V. Jha, B. Krishnamurthy, Modelling the effect of anode particle radius and anode reaction rate constant on capacity fading of Li-ion batteries, *Journal of Electrochemical Science and Engineering* **12(2)** (2022) 359-372. https://doi.org/10.5599/jese.1147 .

[19] J. C. Barbosa, J. P Dias, S. Lanceros-Méndez, C. M. Costa, Recent Advances in Poly (vinylidene fluoride) and Its Copolymers for Lithium-Ion Battery Separators, *Membranes* **8** (2018) 45. https://doi.org/10.3390/membranes8030045

[20] W. Wu, X. Xiao, X. Huang, The effect of battery design parameters on heat generation and utilization in a Li-ion cell, *Electrochimica Acta* **83** (2012) 227-240. https://doi.org/10.1016/j.electacta.2012.07.081

[21] J. Kang, Y. Jia, G. Zhu, J. V. Wang, B. Huang, Y. Fan, How electrode thicknesses influence performance of cylindrical lithium-ion batteries, *Journal of Energy Storage* **46** (2022) 103827. https://doi.org/10.1016/j.est.2021.103827

[22] J. I. Madsen, W. Shyy, R. T. Haftka, Response Surface Techniques for Diffuser Shape Optimization, *AIAA Journal* **38(9)** (2000) 1512-1518. https://doi.org/10.2514/2.1160
[23] A. H. N Shirazi, M. R. Azadi Kakavand, T. Rabczuk, Numerical Study of Composite Electrode's Particle Size Effect on the Electrochemical and Heat Generation of a Li-Ion Battery, *Journal of Nanotechnology in Engineering and Medicine* **6(4)** (2015) 041003. https://doi.org/10.1115/1.4032012
[24] Y. Jin, B. Zhu,Z. Lu, N. Liu, J. Zhu, Challenges and Recent Progress in the Development of Si Anodes for Lithium-Ion Battery, *Advanced Energy Materials* **7** (2017) 1700715. https://doi.org/10.1002/aenm.201700715
[25] *COMSOL Multiphysics®* v. 5.6., COMSOL AB, Stockholm, Sweden. www.comsol.com
[26] R. Endo, Y. Fujihara, M. Susa, Calculation of density and heat capacity of silicon by molecular dynamics simulation, *High Temperatures-High Pressures* **35/36(5)** (2003) 505-511. http://www.thermophysics.ru/pdf_doc/AutoPlay/Docs/CollectionOfManuscripts/ECTP2005paper139.pdf
[27] V. M. Glazov, A. S. Pashinkin, The thermophysical properties (heat capacity and thermal expansion) of single-crystal silicon*, High Temperature* **39(3)** (2001) 413-419. https://doi.org/10.1023/A:1017562709942
[28] S. M. Sze, K. Kwok Ng, *Physics of Semiconductor Devices*, John Wiley & Sons, Inc. **3** (2006) 790. https://doi.org/10.1002/9780470068328.app7
[29] E. Hosseinzadeh, J. Marco, P. Jennings, The impact of multi-layered porosity distribution on the performance of a lithium-ion battery, *Applied Mathematical Modelling* **61** (2018) 107-123. https://doi.org/10.1016/j.apm.2018.04.001